AIAA SciTech Forum
8-12 January 2024, Orlando, FL
AIAA SCITECH 2024 Forum

10.2514/6.2024-2824

Uncertainty in Wind Estimates, Part 1: Analysis using Generalized Polynomial Chaos

Kenneth C. Gahan*, Jeremy W. Hopwood†, and Craig A. Woolsey‡
Virginia Polytechnic Institute and State University, Blacksburg, VA 24061

Indirect wind estimation onboard unmanned aerial systems (UASs) can be accomplished using existing air vehicle sensors along with a dynamic model of the UAS augmented with additional wind-related states. While many indirect estimation approaches achieve desirable accuracy under the assumption of known system parameters, the effect of parametric uncertainty on wind estimate precision is important and has not been thoroughly investigated. This paper describes the theory and process for using generalized polynomial chaos (gPC) to re-cast the dynamics of a system with non-deterministic parameters as a deterministic system. The concepts are applied to the problem of wind estimation and characterizing the precision of wind estimates over time due to known parametric uncertainties. In the multivariate case presented here, gPC exhibits a computational advantage over Monte Carlo sampling-based methods and produces a deterministic system upon which control and estimation methods can be applied.

I. Introduction

Wind estimation from air vehicle motion is useful for many reasons, including weather forecasting and air traffic management [1]. The ability to estimate wind indirectly (i.e., without specialized instrumentation) is of particular interest due to the increasing ubiquity of small unmanned aerial systems (UASs) [2] and the unobtrusive/low-cost nature of using operational sensors (e.g., air vehicle GPS, accelerometers, and gyroscopes). Generally, these estimation methods can be grouped into two major categories: model-based and model-free. Model-based estimation requires accurate aerodynamic and propulsion models of the aircraft to generate state and wind estimates [3, 4]. Model-based methods are popular because they incorporate knowledge of the vehicle dynamics and they do not require direct measurement of the wind, such as with an air data sensor [5], and are thus readily applied to UASs. Present literature, however, often does not address the uncertainty in wind estimates due to uncertainties in the aircraft model.

Uncertainty refers to how imperfect knowledge is manifested in a system or process model [6]. Uncertainty quantification (UQ) is an estimation of the confidence in the output of that model [7]. Uncertainty is generally categorized as either *aleatory* uncertainty, which is inherent (irreducible) randomness in a system or process, or *epistemic* uncertainty, which is incomplete or inexact (reducible) encoding of the physical system or process into the model [8].

Traditionally, sampling-based methods such as Monte Carlo (MC) analysis have been the primary tool for UQ [9]. In MC analysis, numerous deterministic simulations are used to generate posterior statistical information based on known or assumed *a priori* probability distributions for the uncertain elements of a system. MC for UQ has been applied to many diverse problems such as flutter analysis [7], entry vehicle trajectory prediction [10], and chemical reactions [11], to name a few. Although MC is a reliable method for UQ and, indeed, is often a baseline for other methods, it is computationally expensive, sometimes prohibitively so [7]. To avoid the computational burden of MC analysis, approaches such as design of experiments/response surface methodology (DOE/RSM) are available, where an approximated input/output model is tested with a minimal set of inputs [7]. This method is highly dependent on the proper choice of response surface equation, however, and can yield inaccurate or false information if the equation is not chosen carefully. Neither MC nor DOE/RSM are tractable for real-time applications. As an alternative, we present a method for characterizing the aleatory uncertainty in wind estimates due to imperfect knowledge of the system parameters using generalized Polynomial Chaos (gPC) [12] which overcomes these limitations.

In Section II, we present the aircraft motion model for which we develop the state estimator. In Section III we develop the methods for analyzing the uncertainty in wind estimates. Section IV presents an example using flight test data and multivariate uncertainty. In Section V, we present the results from multivariate analysis. Lastly, in Section VI we present conclusions.

*Ph.D. Candidate, Kevin T. Crofton Department of Aerospace and Ocean Engineering, AIAA Student Member
†Ph.D. Candidate, Kevin T. Crofton Department of Aerospace and Ocean Engineering, AIAA Student Member
‡Professor, Kevin T. Crofton Department of Aerospace and Ocean Engineering, AIAA Associate Fellow

II. Aircraft Motion in Wind

A. Wind Field

Consider an aircraft in a wind velocity field, $\boldsymbol{W}$, that varies in space and time. At an instant of time, the wind velocity that would exist at the aircraft center of gravity (CG) if the aircraft were absent – the apparent wind – is

$$\boldsymbol{w}(t) = \boldsymbol{W}\left(\boldsymbol{X}(t), t\right) \tag{1}$$

where $\boldsymbol{X} = [X_N \;\; X_E \;\; X_D]^\mathsf{T}$ is the north-east-down position of the aircraft CG in an orthonormal Earth-fixed inertial reference frame $\mathcal{F}_\mathrm{I}$ defined by unit vectors $\{\boldsymbol{i}_1, \boldsymbol{i}_2, \boldsymbol{i}_3\}$. The total time derivative of the apparent wind is

$$\frac{\mathrm{d}\boldsymbol{w}}{\mathrm{dt}} = \frac{\partial \boldsymbol{W}\left(\boldsymbol{X}, t\right)}{\partial t} + \frac{\partial \boldsymbol{W}\left(\boldsymbol{X}, t\right)}{\partial \boldsymbol{X}} \frac{\mathrm{d}\boldsymbol{X}}{\mathrm{d}t} \tag{2}$$

Adopting the standard overdot notation for the total time derivative we have

$$\dot{\boldsymbol{w}} = \frac{\partial \boldsymbol{W}}{\partial t} + \frac{\partial \boldsymbol{W}}{\partial \boldsymbol{X}} \dot{\boldsymbol{X}} \tag{3}$$

We adopt the following assumption about the dynamics of the wind field:

Assumption 1

(a) *The wind field evolves slowly compared to the aircraft velocity and is thus considered frozen, consistent with* Taylor*'s hypothesis [13], such that* $\frac{\partial \boldsymbol{W}}{\partial t} = \boldsymbol{0}$.

(b) *The variation of the wind field with position is negligible such that* $\frac{\partial \boldsymbol{W}}{\partial \boldsymbol{X}} = \boldsymbol{0}$.

The above assumption implies that $\dot{\boldsymbol{w}} = \boldsymbol{0}$ and the air relative angular velocity of the aircraft is equal to its angular velocity with respect to inertial space. This assumption, which is consistent with [1, 14], could be relaxed but it simplifies the results presented here.

Assumption 1 may seem incompatible with the motivating challenge of estimating variations in the wind velocity. However, the assumption of a steady, uniform wind field does not impede the model-based filter from adjusting wind velocity estimates based on measurements that reflect wind variations.

B. Nonlinear Equations for Fixed-Wing Aircraft Motion in Wind

Having discussed the dynamics of the wind field in Section II.A, we now briefly present the equations of motion for a fixed-wing aircraft in wind. The reader is directed to [15] and [16] for a full treatment of the derivation. We begin by defining the aircraft body reference frame, $\mathcal{F}_\mathrm{B}$, defined by orthonormal vectors $\{\boldsymbol{b}_1, \boldsymbol{b}_2, \boldsymbol{b}_3\}$ originating at the CG, where $\boldsymbol{b}_1$ points forward, $\boldsymbol{b}_2$ points out the right wing, and $\boldsymbol{b}_3$ completes the right-hand rule. The transformation from $\mathcal{F}_\mathrm{B}$ to $\mathcal{F}_\mathrm{I}$ is given by the rotation matrix

$$\boldsymbol{R}_\mathrm{IB}(\boldsymbol{\Theta}) = e^{[\boldsymbol{e}_3 \times]\psi} e^{[\boldsymbol{e}_2 \times]\theta} e^{[\boldsymbol{e}_1 \times]\phi} \tag{4}$$

where $\boldsymbol{\Theta} = [\phi \;\; \theta \;\; \psi]^\mathsf{T}$ are the aircraft Euler angles, $\boldsymbol{e}_1 = [1\ 0\ 0]^\mathsf{T}$, etc., and $[(\cdot)\times]$ is the skew-symmetric cross product equivalent matrix satisfying $[\boldsymbol{a}\times]\boldsymbol{b} = \boldsymbol{a} \times \boldsymbol{b}$ for 3-vectors $\boldsymbol{a}$ and $\boldsymbol{b}$. Note that $\boldsymbol{R}_\mathrm{BI}(\boldsymbol{\Theta}) := \boldsymbol{R}_\mathrm{IB}^{-1}(\boldsymbol{\Theta}) = \boldsymbol{R}_\mathrm{IB}^\mathsf{T}(\boldsymbol{\Theta})$. The aircraft kinematics are given by

$$\dot{\boldsymbol{X}} = \boldsymbol{R}_\mathrm{IB}(\boldsymbol{\Theta})\boldsymbol{v} \tag{5}$$

$$\dot{\boldsymbol{R}}_\mathrm{IB}(\boldsymbol{\Theta}) = \boldsymbol{R}_\mathrm{IB}(\boldsymbol{\Theta})[\boldsymbol{\omega}\times] \tag{6}$$

where $\boldsymbol{v} = [u \;\; v \;\; w]^\mathsf{T}$ is the velocity with respect to the inertial frame, given in the body frame, and $\boldsymbol{\omega} = [p \;\; q \;\; r]^\mathsf{T}$ is the angular velocity with respect to the inertial frame, expressed in the body frame. The matrix differential equation (6) holds independently of any attitude parameterization, but expanding the equation as written, with $\boldsymbol{R}_\mathrm{IB}$ as given in (4), yields the three conventional Euler angle rate equations:

$$\dot{\boldsymbol{\Theta}} = \boldsymbol{L}_\mathrm{IB}(\boldsymbol{\Theta})\boldsymbol{\omega} = \begin{bmatrix} 1 & \sin\phi\tan\theta & \cos\phi\tan\theta \\ 0 & \cos\phi & -\sin\phi \\ 0 & \sin\phi\sec\theta & \cos\phi\sec\theta \end{bmatrix} \begin{bmatrix} p \\ q \\ r \end{bmatrix} \tag{7}$$

As in [17] we make the assertion that the aerodynamic forces, $\boldsymbol{F}$, and moments, $\boldsymbol{M}$, depend on the velocity of the aircraft relative to the wind. For simplicity, we neglect any dependence of $\boldsymbol{F}$ and $\boldsymbol{M}$ on translational acceleration, such as the plunge acceleration ($\dot{w}$) dependence that often appears in fixed-wing flight dynamic models. Let $\boldsymbol{v}_\mathrm{r} = [u_\mathrm{r} \;\; v_\mathrm{r} \;\; w_\mathrm{r}]^\mathsf{T}$ be the air-relative velocity of the CG expressed in the body frame given by

$$\boldsymbol{v}_\mathrm{r} = \boldsymbol{v} - \boldsymbol{R}_\mathrm{BI}(\boldsymbol{\Theta})\boldsymbol{w} \tag{8}$$

Eq. (8) is known as the wind triangle. From Assumption 1, the air-relative angular velocity of the aircraft is equal to the total angular velocity, $\boldsymbol{\omega}$. Therefore, the aerodynamic force $\boldsymbol{F} = [X, Y, Z]^T$ and moment $\boldsymbol{M} = [L, M, N]^T$ have the general dependence

$$\boldsymbol{F} = \boldsymbol{F}(\boldsymbol{v}_\mathrm{r}, \omega, \boldsymbol{u}), \quad \boldsymbol{M} = \boldsymbol{M}(\boldsymbol{v}_\mathrm{r}, \omega, \boldsymbol{u}) \tag{9}$$

where the input $\boldsymbol{u} = [\delta_T \;\; \delta_a \;\; \delta_e \;\; \delta_\mathrm{r}]^\mathsf{T}$ comprises the throttle, aileron, elevator, and rudder control inputs. We use an aerodynamic model from [18] with non-dimensional coefficients of the form

$$\begin{aligned}
C_X &= X(\bar{q}S)^{-1} &&= C_{X_o} + C_{X_\alpha}\alpha + C_{X_{\alpha^2}}\alpha^2 + C_{X_{\delta_\mathrm{e}}}\delta_\mathrm{e} + C_T\delta_T && \text{(10a)}\\
C_Z &= Z(\bar{q}S)^{-1} &&= C_{Z_o} + C_{Z_\alpha}\alpha + C_{Z_q}\hat{q} && \text{(10b)}\\
C_m &= M(\bar{q}S\bar{c})^{-1} &&= C_{m_o} + C_{m_\alpha}\alpha + C_{m_q}\hat{q} + C_{m_{\delta_\mathrm{e}}}\delta_\mathrm{e} && \text{(10c)}\\
C_Y &= Y(\bar{q}S)^{-1} &&= C_{Y_\beta}\beta + C_{Y_p}\hat{p} + C_{Y_r}\hat{r} + C_{Y_{\delta_\mathrm{a}}}\delta_\mathrm{a} + C_{Y_{\delta_\mathrm{r}}}\delta_\mathrm{r} && \text{(10d)}\\
C_l &= L(\bar{q}Sb)^{-1} &&= C_{l_\beta}\beta + C_{l_p}\hat{p} + C_{l_{\delta_\mathrm{a}}}\delta_\mathrm{a} && \text{(10e)}\\
C_n &= N(\bar{q}Sb)^{-1} &&= C_{n_\beta}\beta + C_{n_r}\hat{r} + C_{n_{\delta_\mathrm{a}}}\delta_\mathrm{a} + C_{n_{\delta_\mathrm{r}}}\delta_\mathrm{r} && \text{(10f)}
\end{aligned}$$

where the propulsion coefficient, C_T, is modeled using information from [19]. Here $\bar{q}$ is dynamic pressure, S is the wing planform area, $\bar{c}$ is mean aerodynamic chord, and b is wing span. Note that, in this section, the overhats ($\hat{}$) indicate nondimensional angular rates. In a change of notation, this symbol will later be used to denote estimates; the distinction will be clear from context. Here the angle-of-attack, α, and angle-of-sideslip, β, define the transformation between the body and wind-relative frames with

$$\alpha = \tan^{-1}\left(\frac{w_\mathrm{r}}{u_\mathrm{r}}\right) \qquad \text{and} \qquad \beta = \sin^{-1}\left(\frac{v_\mathrm{r}}{V_\mathrm{r}}\right) \tag{11}$$

where $V_\mathrm{r} = \|\boldsymbol{v}_\mathrm{r}\|$. Thus, the well established nonlinear equations of motion [15, 20], adapted for the assumed wind field, are

$$\begin{aligned}
\dot{\boldsymbol{X}} &= \boldsymbol{R}_\mathrm{IB}(\boldsymbol{\Theta})\boldsymbol{v}_\mathrm{r} + \boldsymbol{w} && \text{(12a)}\\
\dot{\boldsymbol{\Theta}} &= \boldsymbol{L}_\mathrm{IB}(\boldsymbol{\Theta})\omega && \text{(12b)}\\
\dot{\boldsymbol{v}}_\mathrm{r} &= \boldsymbol{v}_\mathrm{r} \times \omega + g\boldsymbol{R}_\mathrm{BI}(\boldsymbol{\Theta})\boldsymbol{e}_3 + \frac{1}{m}\boldsymbol{F}(\boldsymbol{v}_\mathrm{r}, \omega, \boldsymbol{u}) && \text{(12c)}\\
\dot{\omega} &= \boldsymbol{I}^{-1}(\boldsymbol{I}\omega \times \omega) + \boldsymbol{I}^{-1}\boldsymbol{M}(\boldsymbol{v}_\mathrm{r}, \omega, \boldsymbol{u}) && \text{(12d)}
\end{aligned}$$

where $\boldsymbol{I}$ is the aircraft moment of inertia tensor defined at the CG in $\mathcal{F}_B$. At last, we define the aircraft state and measurement equations

$$\begin{aligned}
\dot{\boldsymbol{x}} &= \boldsymbol{f}(\boldsymbol{x}, \boldsymbol{u}, \boldsymbol{w}) && \text{(13a)}\\
\boldsymbol{y} &= \boldsymbol{h}(\boldsymbol{x}, \boldsymbol{u}) && \text{(13b)}
\end{aligned}$$

where the state, input, and wind vectors are

$$\boldsymbol{x} = \begin{bmatrix}\boldsymbol{X}^\mathsf{T} & \boldsymbol{\Theta}^\mathsf{T} & \boldsymbol{v}_\mathrm{r}^\mathsf{T} & \omega^\mathsf{T}\end{bmatrix}^\mathsf{T}, \qquad \boldsymbol{u} = \begin{bmatrix}\delta_T & \delta_a & \delta_e & \delta_\mathrm{r}\end{bmatrix}^\mathsf{T}, \qquad \boldsymbol{w} = \begin{bmatrix}w_N & w_E & w_D\end{bmatrix}^\mathsf{T} \tag{14}$$

where the subscripts N, E, and D are north, east, and down, respectively. We will now present the linearized equations of motion for the aircraft in a wind field.

C. Linear, Small Perturbation Equations for Fixed-Wing Aircraft Motion in Wind

For the purpose of estimating the wind, it is assumed that the aircraft state of motion remains in the neighborhood of a nominal, equilibrium flight condition over a desired time or distance. This nominal flight condition is defined with regard to the *mean* wind field. We let the subscript $\mathbf{eq} = \{(\boldsymbol{x}_\mathrm{e},\ \boldsymbol{u}_\mathrm{e},\ \boldsymbol{w}_\mathrm{e}) \mid \boldsymbol{x}_\mathrm{e} = \boldsymbol{u}_\mathrm{e} = \boldsymbol{w}_\mathrm{e} = \boldsymbol{0}\}$ denote the state and control variables and the mean wind velocity corresponding to a given, equilibrium flight condition (e.g., straight and level cruise in still air). Having defined a nominal, equilibrium state of motion, and assuming that the flight dynamic model is exact, any perturbations from the equilibrium flight condition that are not attributed to the initial state or control inputs can be ascribed to the wind disturbance.

To prepare for the formulation of a state estimator, it is necessary to develop a linear time-invariant (LTI) model from the equations of motion given in Section II.B. Define

$$\boldsymbol{A} = \left.\frac{\partial \boldsymbol{f}}{\partial \boldsymbol{x}}\right|_{\mathbf{eq}} \qquad \boldsymbol{B} = \left.\frac{\partial \boldsymbol{f}}{\partial \boldsymbol{u}}\right|_{\mathbf{eq}} \qquad \boldsymbol{\Pi} = \left.\frac{\partial \boldsymbol{f}}{\partial \boldsymbol{w}}\right|_{\mathbf{eq}} \tag{15}$$

Linearizing the time-invariant system (12) about the equilibrium flight condition gives the LTI system

$$\Delta\dot{\boldsymbol{x}}(t) = \boldsymbol{A}\Delta\boldsymbol{x}(t) + \boldsymbol{B}\Delta\boldsymbol{u}(t) + \boldsymbol{\Pi}\Delta\boldsymbol{w}(t), \qquad \Delta\boldsymbol{x}(0) = \Delta\boldsymbol{x}_{\mathbf{0}} \tag{16a}$$

$$\Delta\boldsymbol{y}(t) = \boldsymbol{C}\Delta\boldsymbol{x}(t) + \boldsymbol{D}\Delta\boldsymbol{u}(t) \tag{16b}$$

where $\Delta\boldsymbol{x} \in \mathbb{R}^{n_x}$, $\Delta\boldsymbol{u} \in \mathbb{R}^{n_u}$, and $\Delta\boldsymbol{w} \in \mathbb{R}^{n_w}$ are perturbations from the equilibrium state, control, and wind vectors. Note that while the position and heading variables in $\boldsymbol{x}_\mathrm{e}$ depend on time, they are ignorable coordinates in the dynamic equations and the resulting small perturbation model is LTI. For brevity, we will drop the Δ notation. In reality the system described by Eq. (16) may be subject to process and/or measurement noise. For simplicity we will proceed without including noise terms. Thus, any discrepancy between the true state, $\boldsymbol{x}$, and the state predicted by the model, $\boldsymbol{x}_\mathrm{e} + \Delta\boldsymbol{x}$, is attributed to uncertainty in the original nonlinear model and to approximation error due to linearization.

III. Wind Estimation and Uncertainty

As described in Section II, a typical process for developing the linear aircraft model needed for wind estimation is to first postulate a nonlinear model structure, then identify the model parameters from experimentation, and lastly linearize about a desired condition. During the system identification process parametric uncertainty can largely be viewed as epistemic. That is, by gathering additional data or considering different model structures, with additional time and effort we could reduce the model uncertainty. Commonly used system identification processes [21, Ch. 6] aim at determining a model structure and model parameters for which the model prediction error is purely random. This purely random error is typically attributed to random disturbances and measurement noise in the output data used for model identification, but a direct consequence is a non-deterministic model in which the model parameters are described by probability distributions (e.g., mean and variance). For this reason, we consider the parameter uncertainty to be well described as aleatory.

This section describes the process of using gPC to characterize the aleatory uncertainty in wind estimates due to the stochastic nature of the linear model matrices.

A. Mapping from Nonlinear Uncertainty to Linear Uncertainty

We first note that the nonlinear equations $\boldsymbol{f}$ can be separated into kinematic and dynamic equations, $\boldsymbol{f} = [\boldsymbol{f}_\mathrm{k}^\mathsf{T}\ \ \boldsymbol{f}_\mathrm{d}^\mathsf{T}]^\mathsf{T}$ respectively. In this work we seek to address the uncertainty in the dynamic equations, $\boldsymbol{f}_\mathrm{d}$, that arises from the aerodynamic parameters ($\boldsymbol{\vartheta} \in \mathbb{R}^m$) given in Table 5. The aerodynamic model (Eq. (10) is linear in its parameters. This is a common choice of model structure [21, Ch. 4]. Thus, the dynamic equations can be further separated into parts independent of and dependent upon $\boldsymbol{\vartheta}$:

$$\boldsymbol{f}_\mathrm{d}(\boldsymbol{x}, \boldsymbol{u}, \boldsymbol{\vartheta}) = \bar{\boldsymbol{f}}_\mathrm{d}(\boldsymbol{x}, \boldsymbol{u}) + \sum_{i=1}^{m} \bar{\boldsymbol{g}}_i(\boldsymbol{x}, \boldsymbol{u})\vartheta_i \tag{17}$$

We can similarly separate $\boldsymbol{A}$, $\boldsymbol{B}$, and $\boldsymbol{\Pi}$ into kinematic and dynamic components:

$$\boldsymbol{A} = \begin{bmatrix} \boldsymbol{A}_\mathrm{k} \\ \boldsymbol{A}_\mathrm{d} \end{bmatrix}, \quad \boldsymbol{B} = \begin{bmatrix} \boldsymbol{B}_k \\ \boldsymbol{B}_\mathrm{d} \end{bmatrix}, \quad \boldsymbol{\Pi} = \begin{bmatrix} \boldsymbol{\Pi}_\mathrm{k} \\ \boldsymbol{\Pi}_\mathrm{d} \end{bmatrix} \tag{18}$$

Then, from Eqs. (15) and (17), the elements of $\boldsymbol{A}_\mathrm{d}$ are

$$A_{\mathrm{d}_{p,q}} = \left.\frac{\partial \bar{f}_{\mathrm{d}_p}}{\partial x_q}\right|_{\mathbf{eq}} + \sum_{i=1}^{m} \left.\frac{\partial \bar{g}_{i,p}}{\partial x_q}\right|_{\mathbf{eq}} \vartheta_i \tag{19}$$

The elements of $\boldsymbol{B}_\mathrm{d}$ and $\boldsymbol{\Pi}_\mathrm{d}$ are found similarly. Equation (19) gives an expression for how uncertainty in the nonlinear model parameters maps to uncertainty in the linear system. To simplify the presentation of gPC, in this work we make the following common assumption [22–24]:

Assumption 2 *The nonlinear model parameters are statistically independent [25].*

Under Assumption 2 we can use Eq. (19), along with knowledge of the nature of the uncertainty of the nonlinear model parameters, to determine the nature of the linear model uncertainties. Referring again to Table 5, the result of the system identification method used to find the nonlinear model parameters [18] is that $\vartheta_i \sim \mathcal{N}(\mu_i, \sigma_i^2)$. Thus, we can apply the *normal sum theorem* [25] to get

$$\mu(A_{\mathrm{d}_{p,q}}) = \left.\frac{\partial \bar{f}_{\mathrm{d}_p}}{\partial x_q}\right|_{\mathbf{eq}} + \sum_{i=1}^{m} \left.\frac{\partial \bar{g}_{i,p}}{\partial x_q}\right|_{\mathbf{eq}} \mu(\vartheta_i) \tag{20}$$

$$\sigma^2(A_{\mathrm{d}_{p,q}}) = \sum_{i=1}^{m} \left(\left.\frac{\partial \bar{g}_{i,p}}{\partial x_q}\right|_{\mathbf{eq}} \sigma(\vartheta_i)\right)^2 \tag{21}$$

We now have

$$\boldsymbol{A}(\boldsymbol{\xi}) = \begin{bmatrix} \boldsymbol{A}_\mathrm{k} \\ \boldsymbol{A}_\mathrm{d}(\boldsymbol{\xi}) \end{bmatrix} \tag{22}$$

where $\boldsymbol{\xi} \in \mathbb{R}^{n_\xi}$ is the vector of random parameters for the linear system. Following similar process we can find $\boldsymbol{B}(\boldsymbol{\xi})$ and $\boldsymbol{\Pi}(\boldsymbol{\xi})$.

B. Augmented System and Filtering

For the purpose of generating wind estimates, we augment the aircraft state vector with the wind states as in [14], defining $\boldsymbol{x}_A = [\boldsymbol{x}^\top\ \boldsymbol{w}^\top]$ so that

$$\dot{\boldsymbol{x}}_A(t) = \begin{bmatrix} \boldsymbol{A} & \boldsymbol{\Pi} \\ \boldsymbol{0} & \boldsymbol{0} \end{bmatrix} \boldsymbol{x}_A(t) + \begin{bmatrix} \boldsymbol{B} \\ \boldsymbol{0} \end{bmatrix} \boldsymbol{u}(t) = \boldsymbol{A}_A \boldsymbol{x}_A(t) + \boldsymbol{B}_A \boldsymbol{u}(t) \tag{23a}$$

$$\boldsymbol{y}_A(t) = \begin{bmatrix} \boldsymbol{C} & \boldsymbol{0} \end{bmatrix} \boldsymbol{x}_A(t) + \boldsymbol{D}\boldsymbol{u}(t) \qquad = \boldsymbol{C}_A \boldsymbol{x}(t) + \boldsymbol{D}\boldsymbol{u}(t) \tag{23b}$$

A Luenberger filter for the augmented system of Eq. (23) is of the form

$$\dot{\hat{\boldsymbol{x}}}_A(t) = \boldsymbol{A}_A \hat{\boldsymbol{x}}_A(t) + \boldsymbol{B}_A \boldsymbol{u}(t) + \boldsymbol{K}\left(\boldsymbol{y}_A(t) - \boldsymbol{C}_A \hat{\boldsymbol{x}}_A(t)\right), \quad \hat{\boldsymbol{x}}_A(0) = \hat{\boldsymbol{x}}_{A_0} \tag{24a}$$

$$\hat{\boldsymbol{z}}(t) = \boldsymbol{L}\hat{\boldsymbol{x}}_A(t) \tag{24b}$$

where the overhat notation, $(\hat{\ })$, now denotes an estimate, $\hat{\boldsymbol{z}}$ are the estimates of interest (e.g., the components of the wind velocity), and $\boldsymbol{K}$ is a generic filter gain matrix that is determined using a method such as Kalman-Bucy filtering or H_∞ filtering [26, 27].

C. Uncertain Filter Equations

Consider the uncertain form of the filter equations (24):

$$\dot{\hat{\boldsymbol{x}}}_A(t,\boldsymbol{\xi}) = \boldsymbol{A}_A(\boldsymbol{\xi}) \hat{\boldsymbol{x}}_A(t,\boldsymbol{\xi}) + \boldsymbol{B}_A(\boldsymbol{\xi}) \boldsymbol{u}(t) + \boldsymbol{K}\left(\boldsymbol{y}_A(t) - \boldsymbol{C}_A \hat{\boldsymbol{x}}_A(t,\boldsymbol{\xi})\right) \tag{25a}$$

$$\hat{\boldsymbol{z}}(t,\boldsymbol{\xi}) = \boldsymbol{L}\hat{\boldsymbol{x}}_A(t,\boldsymbol{\xi}) \tag{25b}$$

Because $\boldsymbol{A}_A$ and $\boldsymbol{B}_A$ are functions of $\boldsymbol{\xi}$, it follows that $\hat{\boldsymbol{x}}_A$ and $\hat{\boldsymbol{z}}$ are stochastic. The matrices $\boldsymbol{C}_A, \boldsymbol{K}$, and $\boldsymbol{L}$ are deterministic. Specifically, $\boldsymbol{C}_A$ and $\boldsymbol{L}$ are determined by available measurements and desired estimates, respectively, and $\boldsymbol{K}$ is designed using some nominal deterministic system.

For these stochastic LTI equations we use gPC to perform generalized polynomial chaos expansion (gPCE) which results in a deterministic system of equations. We then use the resulting gPC system to characterize uncertainty in the wind estimates.

D. Generalized Polynomial Chaos

Let us define a tuple $\boldsymbol{j} = (j_1, \dots, j_{n_\xi}) \in \mathbb{N}_0^{n_\xi}$* with $|\boldsymbol{j}| = j_1 + \cdots + j_{n_\xi}$ denoting the total degree of $\boldsymbol{j}$ [28]. We can construct multivariate gPC basis functions as products of univariate gPC polynomials according to the Weiner-Askey scheme [29]; i.e.,

$$\phi_{\boldsymbol{j}}(\boldsymbol{\xi}) = \phi_{j_1}(\xi_1) \dots \phi_{j_{n_\xi}}(\xi_{n_\xi}), \quad 0 \leq |\boldsymbol{j}| \leq \infty \tag{26}$$

From [30], a second-order random process (i.e., finite variance) can be represented as a gPCE. Thus, for a function $\psi(\boldsymbol{\xi}) : \mathbb{R}^{n_\xi} \to \mathbb{R}$

$$\psi(\boldsymbol{\xi}) = \sum_{|\boldsymbol{j}|=0}^{\infty} \psi_{\boldsymbol{j}} \phi_{\boldsymbol{j}}(\boldsymbol{\xi}) \tag{27}$$

where $\{\psi_{\boldsymbol{j}}\}$ are the expansion coefficients. This expansion converges in the $\mathcal{L}_2$ sense [30, 31]. Fundamental to the concept of gPCE is the orthogonality of basis functions with respect to the distribution $\varphi(\boldsymbol{\xi})$ of $\boldsymbol{\xi}$, where $\varphi(\boldsymbol{\xi}) = \Pi_{k=1}^{n_\xi} \varphi_k(\xi_k)$. That is

$$\left\langle \phi_{\boldsymbol{j}}(\boldsymbol{\xi}), \phi_{\boldsymbol{k}}(\boldsymbol{\xi}) \right\rangle := \int_{\boldsymbol{\Omega}} \phi_{\boldsymbol{j}}(\boldsymbol{\xi}) \phi_{\boldsymbol{k}}(\boldsymbol{\xi}) \varphi(\boldsymbol{\xi}) \mathrm{d}\boldsymbol{\xi} \tag{28a}$$

$$= \mathbb{E}_\xi \{\phi_{\boldsymbol{j}}(\boldsymbol{\xi}) \phi_{\boldsymbol{k}}(\boldsymbol{\xi})\} \tag{28b}$$

$$= \begin{cases} \left\langle \phi_{\boldsymbol{j}}(\boldsymbol{\xi}), \phi_{\boldsymbol{j}}(\boldsymbol{\xi}) \right\rangle, & \text{if } \boldsymbol{j} = \boldsymbol{k} \\ 0, & \text{if } \boldsymbol{j} \neq \boldsymbol{k} \end{cases} \tag{28c}$$

where $\boldsymbol{\Omega}$ is the support of $\varphi(\boldsymbol{\xi})$ given by $\boldsymbol{\Omega} = \Omega_1 \times \cdots \times \Omega_{n_\xi}$ [29]. In practice it is not feasible to perform an exact gPCE, as this requires an infinite number of basis functions. Instead the gPCE is truncated to some suitably high order such that the total degree $|\boldsymbol{j}| \leq p$:

$$\psi(\boldsymbol{\xi}) \approx \sum_{|\boldsymbol{j}|=0}^{p} \psi_{\boldsymbol{j}} \phi_{\boldsymbol{j}}(\boldsymbol{\xi}) =: \tilde{\psi}(\boldsymbol{\xi}) \tag{29}$$

where p is the polynomial order and the number of expansion factors is

$$N_p = \binom{n_\xi + p}{p} := \frac{(n_\xi + p)!}{p!(n_\xi + p - p)!} = \frac{(n_\xi + p)!}{n_\xi! p!} \tag{30}$$

For convenient manipulation of the multi-index $\boldsymbol{j}$, the graded lexicographic order (GLO) is often used [28], where $\boldsymbol{k} > \boldsymbol{j}$ if $|\boldsymbol{k}| > |\boldsymbol{j}|$ or if $|\boldsymbol{k}| = |\boldsymbol{j}|$ and the first nonzero entry in $\boldsymbol{k} - \boldsymbol{j}$ is positive. Table 1 depicts the resulting ordering for a 3-tuple, as well as the associated single-index j'. The orthogonality property expressed in Eq. (28) ensures that $\tilde{\psi}(\boldsymbol{\xi})$ is the minimum error (ϵ) representation of $\psi(\boldsymbol{\xi})$ with respect to the Euclidean norm on the space spanned by the truncated basis functions [32]. This is known as a Galerkin projection [32]. Figure 1 depicts this concept for a two-term gPCE in a single uncertain variable.

E. Galerkin Projection of Stochastic Systems

As in [33], consider a random vector $\boldsymbol{s}^*(t, \boldsymbol{\xi})$ whose n_s components $s_i^*(t, \boldsymbol{\xi})$ are parametrized by $\boldsymbol{\xi}$ for $i \in \{1, \dots, n_s\}$. These components can be approximated using gPCE as follows:

$$s_i^*(t, \boldsymbol{\xi}) \approx \tilde{s}_i(t, \boldsymbol{\xi}) := \sum_{|\boldsymbol{j}|=0}^{p} \underset{\sim}{s}_{i,\boldsymbol{j}}(t) \phi_{\boldsymbol{j}}(\boldsymbol{\xi}) \tag{31}$$

*$\mathbb{N}_0$ are the natural numbers including 0

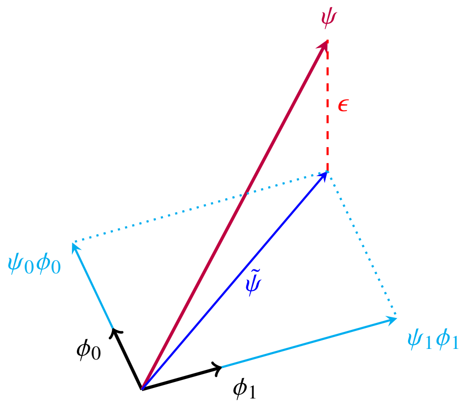

Fig. 1 Galerkin projection of random variable ψ onto the space of two polynomial chaos basis functions ϕ_1 and ϕ_2.

Table 1 Example of graded lexicographic ordering with $n_\xi = 3$.

$\lvert \boldsymbol{j} \rvert$	$\boldsymbol{j}$	j'
0	(0, 0, 0)	0
1	(1, 0, 0)	1
	(0, 1, 0)	2
	(0, 0, 1)	3
2	(2, 0, 0)	4
	(1, 1, 0)	5
	(1, 0, 1)	6
	(0, 2, 0)	7
	(0, 1, 1)	8
	(0, 0, 2)	9
3	(3, 0, 0)	10
	(2, 1, 1)	11
	$\vdots$	$\vdots$

where $\underset{\sim}{s}$ are the gPC expansion coefficients. For compactness, we define

$$\tilde{\boldsymbol{s}}(t,\boldsymbol{\xi}) := \begin{bmatrix} \tilde{s}_1(t,\boldsymbol{\xi}) & \tilde{s}_2(t,\boldsymbol{\xi}) & \dots & \tilde{s}_{n_s}(t,\boldsymbol{\xi}) \end{bmatrix}^\mathsf{T} \in \mathbb{R}^{n_s\times 1} \tag{32a}$$

If $\tilde{\boldsymbol{s}}$ was the state vector for a dynamical system, for example, then $\tilde{s}_1,\dots,\tilde{s}_{n_s}$ would be the individual components, and $\boldsymbol{s}^*(t,\boldsymbol{\xi}) \approx \tilde{\boldsymbol{s}}(t,\boldsymbol{\xi})$. Next we define

$$\underset{\sim}{\boldsymbol{s}}_i(t) := \begin{bmatrix} \underset{\sim}{s}_{i,0}(t) & \underset{\sim}{s}_{i,1}(t) & \dots & \underset{\sim}{s}_{i,j'}(t) \end{bmatrix}^\mathsf{T} \in \mathbb{R}^{N_p\times 1} \tag{32b}$$

which is the column vector of N_p expansion coefficients for a given component of $\tilde{\boldsymbol{s}}$. Additionally, define

$$\boldsymbol{\phi}(\boldsymbol{\xi}) := \begin{bmatrix} \phi_0(\boldsymbol{\xi}) & \phi_1(\boldsymbol{\xi}) & \dots & \phi_{j'}(\boldsymbol{\xi}) \end{bmatrix}^\mathsf{T} \in \mathbb{R}^{N_p\times 1} \tag{32c}$$

which is the column vector of N_p multivariate basis functions corresponding to each expansion coefficient. Lastly, we group the n_s column vectors $\underset{\sim}{\boldsymbol{s}}_i$ to obtain

$$\boldsymbol{s}_{\mathrm{PC}}(t) := \begin{bmatrix} \underset{\sim}{\boldsymbol{s}}_1(t) & \dots & \underset{\sim}{\boldsymbol{s}}_{n_s}(t) \end{bmatrix} \in \mathbb{R}^{N_p\times n_s} \tag{32d}$$

We can now represent the gPCE as

$$\begin{align} \tilde{\boldsymbol{s}}(t,\boldsymbol{\xi}) &= \boldsymbol{s}_{\mathrm{PC}}^\mathsf{T}(t)\boldsymbol{\phi}(\boldsymbol{\xi}) \tag{33a}\\ &= \left(\boldsymbol{\phi}^\mathsf{T}(\boldsymbol{\xi}) \otimes \mathbb{I}_{n_s}\right) \operatorname{vec}\left(\boldsymbol{s}_{\mathrm{PC}}^\mathsf{T}(t)\right) \tag{33b}\\ &=: \Phi_s^\mathsf{T}(\boldsymbol{\xi})\boldsymbol{S}(t) \tag{33c} \end{align}$$

where $\otimes$ is the Kroenecker product and $\operatorname{vec}(\cdot)$ is the vectorization of a matrix [34]. Note that $\Phi_s^\mathsf{T}(\boldsymbol{\xi}) \in \mathbb{R}^{n_s\times n_s N_p}$ and $\boldsymbol{S}(t) \in \mathbb{R}^{n_s N_p\times 1}$.

F. Galerkin Projection of the Uncertain Filter Equations

For clarity, let us use $(\cdot)^*$ to denote the original uncertain filter equation variables (Eq. (25)). Substituting the gPCEs of $\hat{\boldsymbol{x}}_A^*$ and $\hat{\boldsymbol{z}}^*$ into the uncertain filter equations gives

$$\begin{align} \Phi_{\hat{x}_A}^\mathsf{T}(\boldsymbol{\xi})\dot{\hat{\boldsymbol{X}}}_A(t) &= \boldsymbol{A}_A(\boldsymbol{\xi})\Phi_{\hat{x}_A}^\mathsf{T}(\boldsymbol{\xi})\hat{\boldsymbol{X}}_A(t) + \boldsymbol{B}_A(\boldsymbol{\xi})\boldsymbol{u}(t) + \boldsymbol{K}\left(\boldsymbol{y}_A(t) - \boldsymbol{C}_A\Phi_{\hat{x}_A}^\mathsf{T}(\boldsymbol{\xi})\hat{\boldsymbol{X}}_A(t)\right) \tag{34a}\\ \Phi_{\hat{z}}^\mathsf{T}(\boldsymbol{\xi})\hat{\boldsymbol{Z}}(t) &= \boldsymbol{L}\Phi_{\hat{x}_A}^\mathsf{T}(\boldsymbol{\xi})\hat{\boldsymbol{X}}_A(t) \tag{34b} \end{align}$$

Next, multiply the filter equation by $\Phi_{\hat{x}_A}(\boldsymbol{\xi})$ and the estimate equation by $\Phi_{\hat{z}}(\boldsymbol{\xi})$ to get

$$\begin{aligned}\Phi_{\hat{x}_A}(\boldsymbol{\xi})\Phi^{\mathsf{T}}_{\hat{x}_A}(\boldsymbol{\xi})\dot{\hat{\boldsymbol{X}}}_A(t) = \Phi_{\hat{x}_A}(\boldsymbol{\xi})\boldsymbol{A}_A(\boldsymbol{\xi})\Phi^{\mathsf{T}}_{\hat{x}_A}(\boldsymbol{\xi})\hat{\boldsymbol{X}}_A(t) + \Phi_{\hat{x}_A}(\boldsymbol{\xi})\boldsymbol{B}_A(\boldsymbol{\xi})\boldsymbol{u}(t)& \\ + \Phi_{\hat{x}_A}(\boldsymbol{\xi})\boldsymbol{K}\left(\boldsymbol{y}_A(t) - \boldsymbol{C}_A\Phi^{\mathsf{T}}_{\hat{x}_A}(\boldsymbol{\xi})\hat{\boldsymbol{X}}_A(t)\right)& \end{aligned} \tag{35a}$$

$$\Phi_{\hat{z}}(\boldsymbol{\xi})\Phi^{\mathsf{T}}_{\hat{z}}(\boldsymbol{\xi})\hat{\boldsymbol{Z}}(t) = \Phi_{\hat{z}}(\boldsymbol{\xi})\boldsymbol{L}\Phi^{\mathsf{T}}_{\hat{x}_A}(\boldsymbol{\xi})\hat{\boldsymbol{X}}_A(t) \tag{35b}$$

Now, take the expectation of both equations and let $\boldsymbol{M}_{\hat{x}_A} = \mathbb{E}_{\xi}\left\{\Phi_{\hat{x}_A}(\boldsymbol{\xi})\Phi^{\mathsf{T}}_{\hat{x}_A}(\boldsymbol{\xi})\right\}$ and let $\boldsymbol{M}_{\hat{z}} = \mathbb{E}_{\xi}\left\{\Phi_{\hat{z}}(\boldsymbol{\xi})\Phi^{\mathsf{T}}_{\hat{z}}(\boldsymbol{\xi})\right\}$ be the normalization matrices. By Eqs. (28) and (33), $\boldsymbol{M}_{\hat{x}_A}$ and $\boldsymbol{M}_{\hat{z}}$ are diagonal and full rank. Thus,

$$\boldsymbol{M}_{\hat{x}_A}\dot{\hat{\boldsymbol{X}}}_A(t) = \mathcal{A}_A\hat{\boldsymbol{X}}_A(t) + \mathcal{B}_A\boldsymbol{u}(t) + \mathcal{K}\boldsymbol{y}_A(t) - \mathcal{K}C_A\hat{\boldsymbol{X}}_A(t) \tag{36a}$$

$$\boldsymbol{M}_{\hat{z}}\hat{\boldsymbol{Z}}(t) = \mathcal{L}\hat{\boldsymbol{X}}_A(t) \tag{36b}$$

where

$$\mathcal{A}_A = \mathbb{E}_{\xi}\left\{\Phi_{\hat{x}_A}(\boldsymbol{\xi})\boldsymbol{A}_A(\boldsymbol{\xi})\Phi^{\mathsf{T}}_{\hat{x}_A}(\boldsymbol{\xi})\right\} \in \mathbb{R}^{n_{\hat{x}}N_p\times n_{\hat{x}}N_p} \tag{37a}$$

$$\mathcal{B}_A = \mathbb{E}_{\xi}\left\{\Phi_{\hat{x}_A}(\boldsymbol{\xi})\boldsymbol{B}_A(\boldsymbol{\xi})\right\} \in \mathbb{R}^{n_{\hat{x}}N_p\times n_u} \tag{37b}$$

$$\mathcal{K} = \mathbb{E}_{\xi}\left\{\Phi_{\hat{x}_A}(\boldsymbol{\xi})\boldsymbol{K}\right\} \in \mathbb{R}^{n_{\hat{x}}N_p\times n_y} \tag{37c}$$

$$\mathcal{K}C_A = \mathbb{E}_{\xi}\left\{\Phi_{\hat{x}_A}(\boldsymbol{\xi})\boldsymbol{K}\boldsymbol{C}_A\Phi^{\mathsf{T}}_{\hat{x}_A}(\boldsymbol{\xi})\right\} \in \mathbb{R}^{n_{\hat{x}}N_p\times n_{\hat{x}}N_p} \tag{37d}$$

$$\mathcal{L} = \mathbb{E}_{\xi}\left\{\Phi_{\hat{z}}(\boldsymbol{\xi})\boldsymbol{L}\Phi^{\mathsf{T}}_{\hat{x}_A}(\boldsymbol{\xi})\right\} \in \mathbb{R}^{n_{\hat{z}}N_p\times n_{\hat{x}}N_p} \tag{37e}$$

Finally,

$$\dot{\hat{\boldsymbol{X}}}_A(t) = \boldsymbol{M}^{-1}_{\hat{x}_A}\left(\mathcal{A}_A\hat{\boldsymbol{X}}_A(t) + \mathcal{B}_A\boldsymbol{u}(t) + \mathcal{K}\boldsymbol{y}_A(t) - \mathcal{K}C_A\hat{\boldsymbol{X}}_A(t)\right) \tag{38a}$$

$$\hat{\boldsymbol{Z}}(t) = \boldsymbol{M}^{-1}_{\hat{z}}\mathcal{L}\hat{\boldsymbol{X}}_A(t) \tag{38b}$$

where $\hat{\boldsymbol{X}}_A(t) \in \mathbb{R}^{n_{\hat{x}}N_p}$. These gPC filter equations are no longer a function of $\boldsymbol{\xi}$ and are thus deterministic. The outputs are useful for analyzing the statistics of the behavior of the original uncertain system.

G. Statistical Information from the gPC Filter Equations

From the gPCE of Eq. (25) we now have an analytical representation [29, Ch. 5] of the filter equations, Eq. (38), in terms of $\boldsymbol{\xi}$ [29]. From this analytical representation we can directly extract the statistics of the outputs. Recall from Section III.E that

$$\hat{z}^*(t,\boldsymbol{\xi}) \approx \Phi^{\mathsf{T}}_{\hat{z}}(\boldsymbol{\xi})\boldsymbol{Z}(t) \tag{39}$$

The mean of $\hat{z}^*(t,\boldsymbol{\xi})$ over $\boldsymbol{\xi}$ can thus be approximated as

$$\mu_{\hat{z}^*}(t) := \mathbb{E}_{\xi}\{\hat{z}^*(t,\boldsymbol{\xi})\} \approx \mathbb{E}_{\xi}\{\Phi^{\mathsf{T}}_{\hat{z}}(\boldsymbol{\xi})\boldsymbol{Z}(t)\} = \int_{\boldsymbol{\Omega}}\left(\Phi^{\mathsf{T}}_{\hat{z}}(\boldsymbol{\xi})\boldsymbol{Z}(t)\right)\varphi(\boldsymbol{\xi})\mathrm{d}\boldsymbol{\xi} = \boldsymbol{Z}_0(t) \tag{40}$$

Similarly, its covariance, $\Sigma\left(\hat{z}^*(t,\boldsymbol{\xi})\right)$, can be approximated from

$$\begin{aligned}\Sigma\left(\hat{z}^*(t,\boldsymbol{\xi})\right) &= \mathbb{E}_{\xi}\left\{\left(\hat{z}^*(t,\boldsymbol{\xi}) - \mu_{\hat{z}^*}(t)\right)\left(\hat{z}^*(t,\boldsymbol{\xi}) - \mu_{\hat{z}^*}(t)\right)^{\mathsf{T}}\right\} &(41a)\\ &\approx \mathbb{E}_{\xi}\left\{\left(\Phi^{\mathsf{T}}_{\hat{z}}(\boldsymbol{\xi})\boldsymbol{Z}(t) - \boldsymbol{Z}_0(t)\right)\left(\Phi^{\mathsf{T}}_{\hat{z}}(\boldsymbol{\xi})\boldsymbol{Z}(t) - \boldsymbol{Z}_0(t)\right)^{\mathsf{T}}\right\} &(41b)\\ &= \mathbb{E}_{\xi}\left\{\Phi^{\mathsf{T}}_{\hat{z}}(\boldsymbol{\xi})\boldsymbol{Z}(t)\boldsymbol{Z}^{\mathsf{T}}(t)\Phi_{\hat{z}}(\boldsymbol{\xi})\right\} - \boldsymbol{Z}_0(t)\boldsymbol{Z}^{\mathsf{T}}_0(t) &(41c)\\ &= \boldsymbol{M}_{\hat{z}}\boldsymbol{Z}(t)\boldsymbol{Z}^{\mathsf{T}}(t) - \boldsymbol{Z}_0(t)\boldsymbol{Z}^{\mathsf{T}}_0(t) &(41d)\end{aligned}$$

Thus, the total variance of $\hat{z}^*(t,\boldsymbol{\xi})$ is $\sigma^2\left(\hat{z}^*(t,\boldsymbol{\xi})\right) = \mathrm{tr}\left(\Sigma\left(\hat{z}^*(t,\boldsymbol{\xi})\right)\right)$. Other statistical information, such as coskewness or cokurtosis, can be determined similarly [35].

IV. Multivariate Uncertainty Quantification from Flight Test Data

A. Research Aircraft

The research aircraft used in this effort is the My Twin Dream (MTD), shown in Fig. 2, manufactured by My Fly Dream. It is a radio-controlled foam aircraft with counter-rotating twin electric motors and APC 10-in. diameter, 6-in. pitch (10x6) propellers. The aircraft was instrumented with a Cubepilot CubeOrange flight computer running PX4 firmware. The sensors onboard the aircraft include triple-redundant accelerometers and gyroscopes, two magnetometers, a Real-Time Kinematic (RTK) global positioning system (GPS) receiver, and a vaned air data unit for wind estimate validation. The MTD was chosen for its simple construction, propeller location (to accommodate the air data boom), and endurance of approximately 25 minutes.The MTD's physical properties are listed in Table 2. The aerodynamic force and moment coefficients in Eq. (10) are from [18] and are reproduced in Table 5 in Appendix A along with their associated mean (μ), standard deviation (σ), and coefficient of variation (CV) [36]. The propulsion coefficient comes from a model based on the wind tunnel data from [19].

Fig. 2 My Twin Dream (MTD) aircraft

Table 2 My Twin Dream (MTD) properties

Property	Symbol	Value	Units
Mass	m	3.311	kg
Mean aerodynamic chord	$\bar{c}$	0.254	m
Projected wing span	b	1.800	m
Wing planform area	S	0.457	m^2
Roll moment of inertia	I_{xx}	0.319	kg-m^2
Pitch moment of inertia	I_{yy}	0.267	kg-m^2
Yaw moment of inertia	I_{zz}	0.471	kg-m^2
Product of inertia	I_{xz}	0.024	kg-m^2
Product of inertia	I_{xy}, I_{yz}	≈ 0	kg-m^2

The accelerometers, gyroscopes, magnetometers, and GPS feed into an extended Kalman filter as part of the PX4 firmware, from which we use position ($\boldsymbol{X}$), attitude ($\boldsymbol{\Theta}$), and angular velocity ($\boldsymbol{\omega}$), which are provided along with their respective state estimate error variances [37].

The wind estimates were compared to reconstructed wind data from a vaned air data unit (ADU) mounted out the nose of the aircraft as pictured in Figure 2. This sensor was developed, manufactured, and calibrated by the Nonlinear Systems Laboratory at Virginia Tech [26, 27]. It consists of two 3D printed vanes attached to magnetic rotary encoders and a 3D printed Kiel probe connected to a MS5525DSO† pressure sensor. The pulse-width modulation (PWM) rotary encoders are read at a sample rate of 200 Hz by a microcontroller that communicates with the flight computer over the CAN bus via a custom PX4 driver. The pressure sensor is natively supported by PX4 and configured to log calibrated airspeed data at 10 Hz.

Let V, α, and β_f be the airspeed, angle-of-attack, and flank angle reported by the ADU, respectively. By using GPS velocity measurements $\boldsymbol{v}_\mathrm{i}$ (accuracy of 0.05 m/s), autopilot attitude estimates (with quaternion estimate standard deviations $\approx 10^{-3}$), and angular velocity measurements from the calibrated gyroscope (noise and bias removed), the wind velocity may be reconstructed as

$$\boldsymbol{w} = \boldsymbol{v}_\mathrm{i} - \boldsymbol{R}_\mathrm{IB}\left(\boldsymbol{v}_\mathrm{ADU} - \boldsymbol{\omega} \times \boldsymbol{r}_\mathrm{ADU}\right) \tag{42}$$

where

$$\boldsymbol{v}_\mathrm{ADU} = \boldsymbol{R}_\mathrm{BW}(\alpha, \beta)\boldsymbol{e}_1 V_\mathrm{r}$$

Here, $\boldsymbol{v}_\mathrm{ADU}$ is the air-relative velocity at the geometric center of the ADU vanes, whose position in the body frame is denoted $\boldsymbol{r}_\mathrm{ADU}$. The rotation matrix $\boldsymbol{R}_\mathrm{BW}(\alpha, \beta) = e^{-[\boldsymbol{e}_2\times]\alpha} e^{[\boldsymbol{e}_3\times]\beta}$, which maps free vectors from the wind frame to the body frame, is parameterized by the measured angle-of-attack, α, and the sideslip angle, $\beta = \tan^{-1}(\tan(\beta_f)\cos(\alpha))$. The accuracy of the reconstructed wind data can be characterized by propagating the measurement uncertainty through Eq. (42). Due to the low error of the constituent measurements, the reconstructed wind is treated as a truth source for wind estimate validation. This air data unit was validated in the Virginia Tech Aerospace and Ocean Engineering department's open jet wind tunnel both for steady-state readings and dynamic response. The airspeed-dependent cutoff frequencies of the vanes were found to be greater than 16 Hz, well above the fastest rigid body modes, which determine an upper limit on the dynamic response of model-based wind estimators.

†Manufactured by TE Connectivity

B. Flight Test

A flight test campaign was conducted at Virginia Tech's Kentland Experimental Aerial Systems (KEAS) airfield on September 28th, 2022 using the UAS described in Section IV.A. Data were gathered during four passes over the ground control station (referred to as Runs 1-4) at 76 m (250 ft) AGL when the wind conditions at ground level were gusty. Gusty conditions were chosen since the goal is to achieve accurate wind estimates under any condition in which the UAS is able to fly. Since we are utilizing an LTI model we restricted the maneuver to nominally steady flight, namely straight-and-level unaccelerated flight.

C. Computer Specifications

The simulations presented in this section were performed in Matlab R2023b on a laptop with an AMD Ryzen 7 PRO 7840U CPU with eight physical cores and 64 GB of DDR5-6400 memory. The MC simulations were accomplished using Matlab's `parfor` command[‡] and the gPC computations were accomplished analytically using symbolic integration along with `parfor`.

D. Methodology

This first step in computing the gPCE of Section III is to determine how the uncertainty in the nonlinear model parameters, given in Table 5 (Appendix A), maps to uncertainty in the entries of the linear system matrices. This is done analytically according to Section III.A. The resulting statistics for the $\boldsymbol{A}(\boldsymbol{\xi})$ matrix entries are presented in Table 3. Note that only the entries which are affected by changes in aerodynamic parameters, i.e. dynamic states and derivatives, are given. Next, to create the nominal LUENBERGER filter (nom), the filter gain matrix $\boldsymbol{K}_{\text{nom}}$ is found using a deterministic method based on the nominal system, where $\boldsymbol{A}_{\text{nom}} = \mathbb{E}_{\xi}\{\boldsymbol{A}(\boldsymbol{\xi})\}$. For the results shown here, H_∞ filtering as presented in [26, 27] was used. Alternatively, another method such as KALMAN-BUCY filtering, could be used to analyze its uncertainty propagation.

Table 3 Uncertain entries of linear $A(\xi)$ matrix

Axis of Motion	Deriv. (row)	State (col.)	Matrix Entry	Mean (μ)	Std. Dev. (σ)	CV $\left(\frac{\sigma}{\lvert\mu\rvert}\right)$
Longitudinal	$\dot{u}_{\text{r}}(7)$	$u_{\text{r}}(7)$	$A_{7,7}$	-0.197	0.090	0.46
	$\dot{w}_{\text{r}}(9)$	$u_{\text{r}}(7)$	$A_{9,7}$	-0.932	0.276	0.28
	$\dot{q}(11)$	$u_{\text{r}}(7)$	$A_{11,7}$	+0.015	0.066	4.12
		$w_{\text{r}}(9)$	$A_{11,9}$	-2.416	0.147	0.06
		$q(11)$	$A_{11,11}$	-9.684	0.233	0.02
Lateral-Directional	$\dot{v}_{\text{r}}(8)$	$v_{\text{r}}(8)$	$A_{8,8}$	-0.708	0.200	0.28
		$p(10)$	$A_{8,10}$	+0.474	0.207	0.44
		$r(12)$	$A_{8,12}$	-19.64	0.847	0.04
	$\dot{p}(10)$	$v_{\text{r}}(8)$	$A_{10,8}$	-0.997	0.133	0.13
		$p(10)$	$A_{10,10}$	-11.27	1.194	0.11
		$r(12)$	$A_{10,12}$	-0.177	0.043	0.24
	$\dot{r}(12)$	$v_{\text{r}}(8)$	$A_{12,8}$	+1.767	0.440	0.25
		$p(10)$	$A_{12,10}$	-0.574	0.061	0.10
		$r(12)$	$A_{12,12}$	-2.352	0.573	0.24

From Table 3 we identify the matrix entries we would like to analyze. There is no limit to the number of entries that can be included, but the computational burden of performing the gPCE grows with N_p (Eq. (30)). This is commonly referred to as the *curse of dimensionality*. To simplify the results presented here we will only consider the three longitudinal entries with the largest CV from Table 3: $A_{7,7}$, $A_{9,7}$, and $A_{11,7}$. Since the distribution of each stochastic entry is GAUSSIAN, the appropriate gPC polynomial basis is the family of HERMITE polynomials [29], given by

$$\text{He}_n(\xi) = (-1)^n e^{\frac{\xi^2}{2}} \frac{\text{d}^{\text{n}}}{\text{d}\xi^{\text{n}}} e^{\frac{-\xi^2}{2}} \tag{43}$$

[‡] https://www.mathworks.com/products/parallel-computing.html

The first five Hermite polynomials are

$$\mathrm{He}_0 = 1,\ \mathrm{He}_1 = \xi,\ \mathrm{He}_2 = \xi^2 - 1,\ \mathrm{He}_3 = \xi^3 - 3\xi,\ \mathrm{He}_4 = \xi^4 - 6\xi^2 + 3 \tag{44}$$

with the corresponding probability density function

$$\varphi(\xi) = \frac{1}{\sqrt{2\pi}} e^{-\frac{\xi^2}{2}}, \quad \text{with support } \Omega = (-\infty, \infty) \tag{45}$$

Recalling Section III.D, we are not constrained to an assumption of normality to apply gPC. But, given the nature of the the uncertainties being considered, Gauss-Hermite polynomials are appropriate. Using the three chosen uncertain longitudinal entries, MC simulations were conducted and gPC was performed to compare the computational cost and accuracy of the two methods. For the MC simulations the filter gain matrix $\boldsymbol{K}_{\text{nom}}$ does not change. Only the state matrix changes to capture the uncertainty between the "actual" aircraft dynamics and the "assumed" dynamics used in the filter. The variation in the set of estimates $\{\hat{w}_N,\ \hat{w}_E,\ \hat{w}_D\}$ in Section V are a result of the uncertainty in the state matrix, $\boldsymbol{A}(\boldsymbol{\xi})$, which was ignored in the design of the filter. Thus, the form of the filter equations used for the MC simulations was

$$\dot{\hat{\boldsymbol{x}}}_A(t,\boldsymbol{\xi}) = \boldsymbol{A}_A(\boldsymbol{\xi})\hat{\boldsymbol{x}}_A(t,\boldsymbol{\xi}) + \boldsymbol{B}_A\boldsymbol{u}(t) + \boldsymbol{K}_{\text{nom}}\left(\boldsymbol{y}_A(t) - \boldsymbol{C}_A\hat{\boldsymbol{x}}_A(t,\boldsymbol{\xi})\right) \tag{46a}$$

$$\hat{z}(t,\boldsymbol{\xi}) = \boldsymbol{L}\hat{\boldsymbol{x}}_A(t,\boldsymbol{\xi}) \tag{46b}$$

Since MC results are used as a baseline for evaluating the gPC results, we must ensure that the MC simulations have converged. By "converged" we mean that a sufficient number of simulations have been conducted to accurately capture the uncertainty in the output. Using the variance in the filter estimates as the quantity of interest, for the results presented we used a doubling scheme for the number of MC simulations, N_{MC}, and continued until the change in variance, $\Delta\sigma^2_{\text{MC}}$, from N_{MC} to $2N_{\text{MC}}$ was less than a desired percentage. Since MC converges at a rate $O\left(N_{\text{MC}}^{-1/2}\right)$ [38], this double and check scheme was seen as a favorable method to establish the MC baseline.

V. Results

The MC simulation convergence criterion $\Delta\sigma^2_{\text{MC}}$ was chosen as 1%, which required 255,000 simulations. Figure 3 shows the MC simulations of the nominal filter (Eq. (46)) allowing for uncertainty in the three selected longitudinal entries of $\boldsymbol{A}(\boldsymbol{\xi})$. Since for this particular test case the aircraft was flown on a north-south course (see Figure 4) we would expect the longitudinal uncertainty to manifest as uncertainty in the north wind component. As can be seen the north component, $\hat{w}_N$, is affected the most by these uncertainties (i.e., it has the largest variance in estimates over time), followed by the east component, $\hat{w}_E$. The downward component, $\hat{w}_D$, is much less affected. For reference the actual wind values $(w_N,\ w_E,\ w_D)$ measured by the ADU discussed in Section IV.A are also shown.

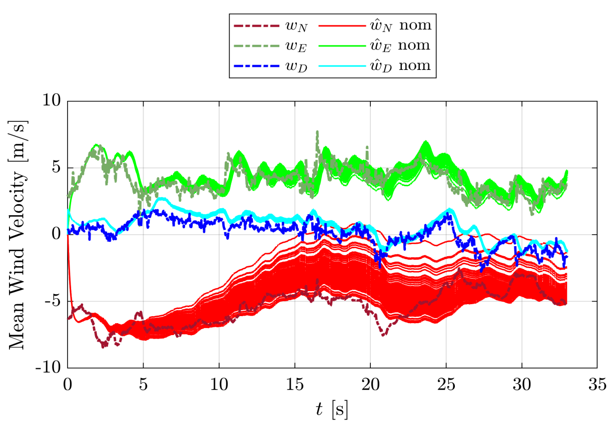

Fig. 3 Monte Carlo simulations of the nominal filter with uncertainty in the longitudinal entries of $A(\xi)$.

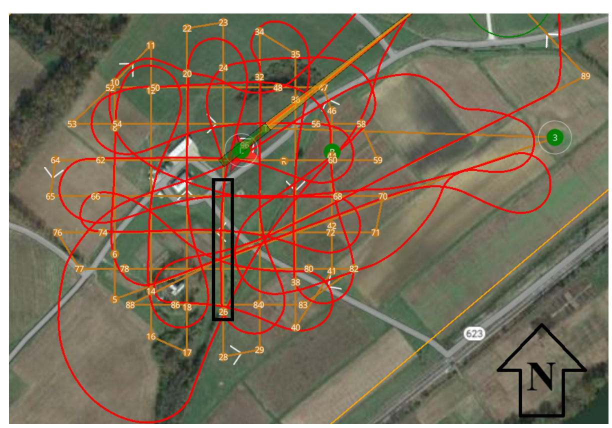

Fig. 4 Test flight path (results data segment outlined in black).

Table 4 presents the computation times for the MC and gPC simulations, as well as the average and maximum error in variance between the gPC approximations and the MC baseline data for $\hat{w}_N$. Error is defined as $\epsilon\left(\sigma^2\right) = \sigma^2_{\text{MC}} - \sigma^2_{\text{PCE}}$.

Table 4 Computation time and error for gPC of increasing orders with $n_\xi = 3$, $(A_{7,7}, A_{9,7}, A_{11,7})$

					$\epsilon\left(\sigma^2(\hat{w}_N)\right)$			
		Computation Time [mm:ss.s]			Average		Maximum	
Method	Simulations	gPC	Simulation	Total	[m^2/s^2]	%	[m^2/s^2]	%
Monte Carlo	255000	N/A	08:38.1	08:38.1	–	–	–	–
1st order gPCE (p = 1)	1	00:04.7	00:00.1	00:04.8	0.049	13.1	0.115	15.1
2nd order gPCE (p = 2)	1	00:45.2	00:00.2	00:45.4	0.003	0.8	0.008	1.0
3rd order gPCE (p = 3)	1	05:47.6	00:00.8	05:48.4	<0.001	<0.1	<0.001	<0.1

It can be seen that a 2nd order gPCE accurately captures the variance in $\hat{w}_N$ due to uncertainty in $\boldsymbol{A}(\boldsymbol{\xi})$ while achieving a 92% reduction in computation time. The 3rd order gPCE requires significantly more computation time for marginal improvements. Figure 5 shows that all three orders of gPCE that were tested can accurately track the MC mean wind. This is expected because, recalling Eq. (40), the mean wind is given by the zeroth gPC expansion coefficient of each wind component.

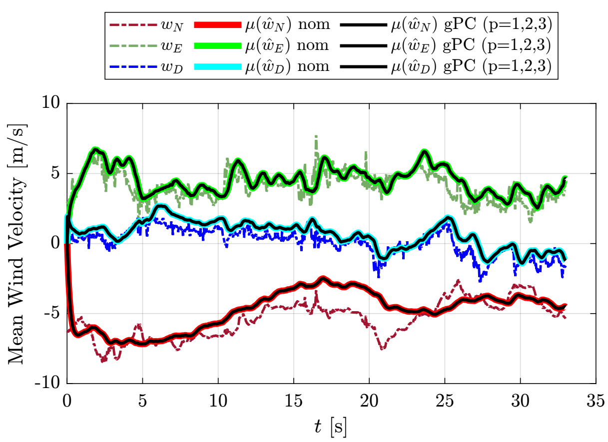

Fig. 5 Mean wind velocities from MC of nominal filter and single runs of gPC filters of different orders.

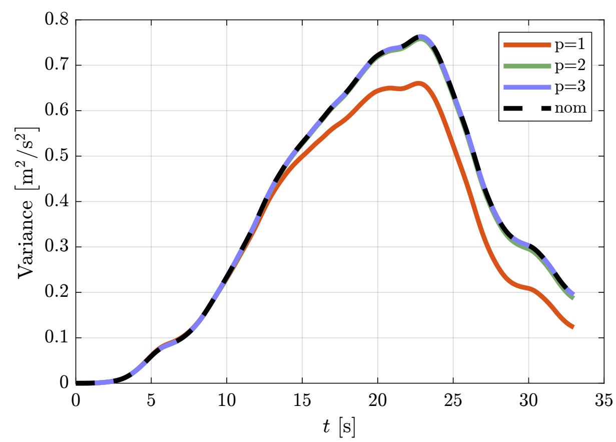

Fig. 6 Variance in $\hat{w}_N$ calculated from MC of nominal filter and single runs of gPC filters of different orders.

Figures 6-8, in contrast, show the improvement in variance tracking as the gPCE order increases. Note that the green curve, representing the 2nd order gPCE, is obscured by the blue curve since their values are nearly identical. In general, the rate of convergence of gPCE orders is dictated by the compatibility of the random parameters with the chosen basis functions and whether the system depends smoothly on the random parameters [29, Ch. 3]. For the results presented here the uncertainties in $\boldsymbol{A}(\boldsymbol{\xi})$ are well-represented by Hermite polynomials and the filter equations smoothly depend on $\boldsymbol{A}(\boldsymbol{\xi})$. Thus, here a 2nd order gPCE is sufficient.

VI. Conclusions and Comments

This paper describes the theory and process for obtaining a deterministic system of equations from a stochastic system using gPC. The concepts are applied to the problem of model-based wind estimation using measurements obtained from an unmanned aircraft. The aim is to obtain a measure of the precision of these wind estimates over time, given known uncertainties in model parameters. For the multivariate case presented here, gPC shows computational advantages over MC sampling-based methods. Additionally, in practice the gPCE could be computed offline and the resulting system of equations used in real-time applications, such as in a synthetic air data system or path planning algorithm, which is not possible using MC. The methods presented here are extensible to nonlinear systems [22] and interdependent uncertainties [39, 40], so the applications of gPC are manifold. In Part 2 of this two part series [41], we demonstrate the use of gPC and H_∞ filtering to reduce the uncertainty in wind estimates.

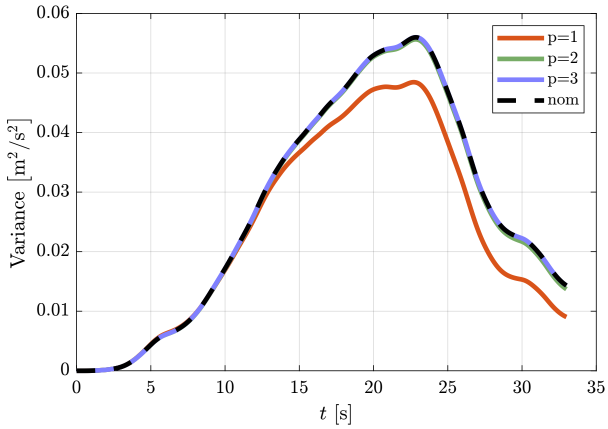

Fig. 7 Variance in $\hat{w}_E$ calculated from MC of nominal filter and single runs of gPC filters of different orders.

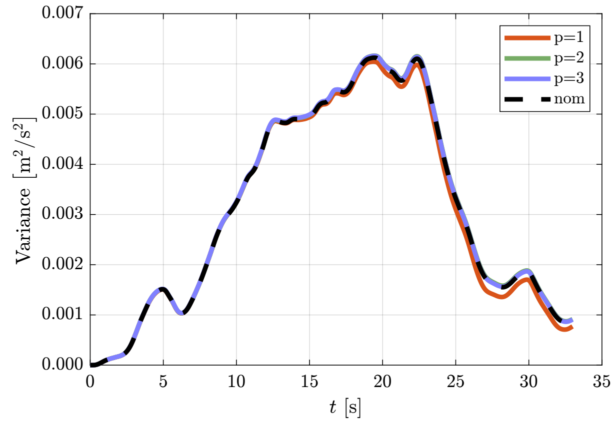

Fig. 8 Variance in $\hat{w}_D$ calculated from MC of nominal filter and single runs of gPC filters of different orders.

Appendix A. Nonlinear Model Parameters

Table 5 Nonlinear Model Parameters [18]

Axis of Motion	Coefficient	Parameter (ϑ_i)	Mean ($\mu(\vartheta_i)$)	Std. Dev. ($\sigma(\vartheta_i)$)	CV $\left(\frac{\sigma}{\lvert\mu\rvert}\right)$
Longitudinal	C_X	C_{X_0}	+0.009	0.026	2.89
		C_{X_α}	+0.282	0.000	0.00
		$C_{X_{\alpha^2}}$	+3.173	0.119	0.04
		$C_{X_{\delta_e}}$	+0.051	0.025	0.49
	C_Z	C_{Z_0}	-0.255	0.074	0.29
		C_{Z_α}	-4.436	0.015	0.00
		C_{Z_q}	-12.54	0.030	0.00
	C_m	C_{m_0}	+0.008	0.006	0.75
		C_{m_α}	-0.444	0.027	0.06
		C_{m_q}	-14.02	0.336	0.02
		$C_{m_{\delta_e}}$	-0.415	0.058	0.14
Lateral-Directional	C_Y	C_{Y_β}	-0.410	0.115	0.28
		C_{Y_p}	+0.221	0.133	0.60
		C_{Y_r}	+0.230	0.547	2.38
		$C_{Y_{\delta_a}}$	+0.118	0.011	0.09
		$C_{Y_{\delta_r}}$	+0.136	0.030	0.22
	C_l	C_{l_β}	-0.035	0.004	0.11
		C_{l_p}	-0.386	0.041	0.11
		$C_{l_{\delta_a}}$	-0.137	0.010	0.07
	C_n	C_{n_β}	+0.083	0.020	0.24
		C_{n_r}	-0.119	0.029	0.24
		$C_{n_{\delta_a}}$	+0.013	0.009	0.69
		$C_{n_{\delta_r}}$	-0.068	0.006	0.09

Acknowledgements

The authors thank Mekonen H. Halefom[§] for his support during flight test activities. The authors also gratefully acknowledge the sponsorship of NASA under Grant No. 80NSSC20M0162 as well as the support of the U.S. Air Force and Virginia Tech's Kevin T. Crofton Department of Aerospace and Ocean Engineering.

[§]Ph.D. Candidate, Kevin T. Crofton Department of Aerospace and Ocean techniques Engineering, AIAA Student Member

References

[1] González-Rocha, J., De Wekker, S. F. J., Ross, S. D., and Woolsey, C. A., "Wind Profiling in the Lower Atmosphere from Wind-Induced Perturbations to Multirotor UAS," *Sensors*, Vol. 20, No. 5, 2020. https://doi.org/10.3390/s20051341.

[2] Fuhrmann, M., and Horowitz, M. C., "Droning on: Explaining the Proliferation of Unmanned Aerial Vehicles," *International Organization*, Vol. 71, No. 2, 2017, pp. 397–418. https://doi.org/10.1017/S0020818317000121.

[3] Lie, F., and Gebre-Egziabher, D., "Synthetic Air Data System," *Journal of Aircraft*, Vol. 50, 2013, pp. 1234–1249. https://doi.org/10.2514/1.C032177.

[4] Lee, J. H., Sevil, H., Dogan, A., and Hullender, D., "Estimation of Maneuvering Aircraft States and Time-Varying Wind with Turbulence," *AIAA Guidance, Navigation, and Control Conference*, Minneapolis, MN, 2012. https://doi.org/10.2514/6.2012-4532.

[5] Ahmed, Z., Halefom, M. H., and Woolsey, C. A., "A Survey of Wind Estimation Methods using Small Uncrewed Aerial Vehicles," *(In review.)*, 2023.

[6] Mcmanus, H. L., and Hastings, D. E., "A Framework for Understanding Uncertainty and its Mitigation and Exploitation in Complex Systems," *IEEE Engineering Management Review*, Vol. 34, No. 3, 2006, pp. 81–81. https://doi.org/10.1109/EMR.2006.261384.

[7] Danowsky, B. P., Chrstos, J. R., Klyde, D. H., Farhat, C., and Brenner, M., "Evaluation of Aeroelastic Uncertainty Analysis Methods," *Journal of Aircraft*, Vol. 47, No. 4, 2010, pp. 1266–1273. https://doi.org/10.2514/1.47118.

[8] Kiureghian, A. D., and Ditlevsen, O., "Aleatory or epistemic? Does it matter?" *Structural Safety*, Vol. 31, No. 2, 2009, pp. 105–112. https://doi.org/10.1016/j.strusafe.2008.06.020.

[9] Kroese, D. P., Brereton, T., Taimre, T., and Botev, Z. I., "Why the Monte Carlo method is so important today," *WIREs Computational Statistics*, Vol. 6, No. 6, 2014, pp. 386–392. https://doi.org/10.1002/wics.1314.

[10] Dutta, S., and Braun, R. D., "Statistical Entry, Descent, and Landing Performance Reconstruction of the Mars Science Laboratory," *Journal of Spacecraft and Rockets*, Vol. 51, No. 4, 2014, pp. 1048–1061. https://doi.org/10.2514/1.A32937.

[11] Albert, D. R., "Monte Carlo Uncertainty Propagation with the NIST Uncertainty Machine," *Journal of Chemical Education*, Vol. 97, No. 5, 2020, pp. 1491–1494. https://doi.org/10.1021/acs.jchemed.0c00096.

[12] Xiu, D., and Karniadakis, G. E., "Modeling uncertainty in flow simulations via generalized polynomial chaos," *Journal of Computational Physics*, Vol. 187, No. 1, 2003, pp. 137–167. https://doi.org/10.1016/S0021-9991(03)00092-5.

[13] Stull, R., "Mean Boundary Layer Characteristics," *An Introduction to Boundary Layer Meteorology*, Kluwer Academic Publishers, Dordrecht, The Netherlands, 1988, pp. 5–6. https://doi.org/10.1007/978-94-009-3027-8.

[14] González-Rocha, J., Woolsey, C. A., Sultan, C., and De Wekker, S. F. J., "Sensing Wind from Quadrotor Motion," *Journal of Guidance, Control, and Dynamics*, Vol. 42, No. 4, 2019, pp. 836–852. https://doi.org/10.2514/1.G003542.

[15] Etkin, B., "General Equations of Unsteady Motion," *Dynamics of Atmospheric Flight*, John Wiley and Sons, New York, 1972, pp. 121–157.

[16] Frost, W., and Bowles, R. L., "Wind Shear Terms in the Equations of Aircraft Motion," *Journal of Aircraft*, Vol. 21, No. 11, 1984, pp. 866–872. https://doi.org/10.2514/3.45056.

[17] McClelland, H. G., and Woolsey, C. A., "Effects of Two Modeling Assumptions on Wind Reconstruction from Longitudinal Aircraft Motion," *Journal of Guidance, Control, and Dynamics*, Vol. 43, No. 6, 2020, pp. 1069–1081. https://doi.org/10.2514/1.G004224.

[18] Halefom, M. H., Gresham, J. L., and Woolsey, C. A., "Modeling and System Identification of Unsteady Aerodynamic Parameters for a Small Fixed-wing Aircraft," *(In preparation.)*, 2023.

[19] Brandt, J., Deters, R., Ananda, G., Dantsker, O., and Selig, M., "UIUC Propeller Database,Vols 1-4," , Nov 2022. Retrieved from https://m-selig.ae.illinois.edu/props/propDB.html.

[20] Yechout, T. R., "Aircraft Equations of Motion," *Introduction to Aircraft Flight Mechanics*, AIAA Education Series, American Institute of Aeronautics & Astronautics, Reston, VA, 2014, 2nd ed., pp. 163–192. https://doi.org/10.2514/4.102547.

[21] Morelli, E. A., and Klein, V., *Aircraft System Identification: Theory and Practice*, 2^{nd} ed., Sunflyte Enterprises, Williamsburg, VA, 2016. ISBN:978-0-9974306-1-5.

[22] de Freitas Virgilio Pereira, M., "Polynomial Chaos-based Control Design for an Aircraft at High Angles of Attack with Uncertain Aerodynamics," Ph.D. thesis, Instituto Tecnologico de Aeronautica, 2017.

[23] Xu, Y., "Uncertainty Quantification, State, and Parameter Estimation in Power Systems using Polynomial Chaos Based Methods," Ph.D. thesis, Virginia Polytechnic Institute and State University, 2020.

[24] Walters, G., "Application of Generalized Polynomial Chaos to Flow-Induced Vibration and Sound," Ph.D. thesis, The Pennsylvania State University, 2020.

[25] Lemons, D. S., *An Introduction to Stochastic Processess in Physics*, Springer Finance Textbooks, Johns Hopkins University Press, 2002. ISBN:0-8018-6866-1.

[26] Gahan, K. C., Hopwood, J. W., and Woolsey, C. A., "Wind Estimation using an H_∞ Filter with Fixed-Wing Aircraft Flight Test Results," *AIAA SCITECH 2023 Forum*, National Harbor, MD, 2023. https://doi.org/10.2514/6.2023-2252.

[27] Gahan, K. C., Hopwood, J. W., and Woolsey, C. A., "Wind Estimation using an H_∞ Filter with Fixed-Wing Aircraft Flight Test Results," *(In review.)*, 2023.

[28] Cox, D., Little, J., and O'Shea, D., *Ideals, Varieties, and Algorithms: An Introduction to Computational Algebraic Geometry and Commutative Algebra*, 4^{th} ed., Springer Int'l Publishing, Switzerland, 2015, Chap. 2. https://doi.org/10.1007/978-3-319-16721-3.

[29] Xiu, D., "Generalized Polynomial Chaos," *Numerical Methods for Stochastic Computations: A Spectral Method Approach*, Princeton University Press, 2010, pp. 57–67. https://doi.org/10.5555/1893088.

[30] Xiu, D., and Karniadakis, G. E., "The Wiener–Askey Polynomial Chaos for Stochastic Differential Equations," *SIAM Journal on Scientific Computing*, Vol. 24, No. 2, 2002, p. 619–644. https://doi.org/10.1137/s1064827501387826.

[31] Cameron, R. H., and Martin, W. T., "The Orthogonal Development of Non-linear Functionals in Series of Fourier-Hermite Functionals," *The Annals of Mathematics*, Vol. 48, No. 2, 1947, p. 385. https://doi.org/10.2307/1969178.

[32] Debusschere, B., "Intrusive Polynomial Chaos Methods for Forward Uncertainty Propogation," *Handbook of Uncertainty Quantification*, edited by R. Ghanem, D. Higdon, and H. Owhadi, Springer Int'l Publishing, Switzerland, 2017, Chap. 17, pp. 617–636. https://doi.org/10.1007/978-3-319-11259-6.

[33] Wan, Y., Shen, D. E., Lucia, S., Findeisen, R., and Braatz, R. D., "Robust static $\mathcal{H}_\infty$ output-feedback control using Polynomial Chaos," *2018 Annual American Control Conference (ACC)*, Milwaukee, WI, 2018. https://doi.org/10.23919/acc.2018.8431074.

[34] Horn, R. A., and Johnson, C. R., *Matrix Analysis*, Cambridge University Press, 1985. https://doi.org/10.1017/CBO9780511810817.

[35] Meucci, A., *Risk and Asset Allocation*, Springer Finance Textbooks, Springer, 2009, Chap. 2. https://doi.org/10.1007/978-3-540-27904-4.

[36] Everitt, B., and Skrondal, A., *The Cambridge Dictionary of Statistics*, Cambridge University Press, 2010. https://doi.org/10.1111/j.1751-5823.2011.00149_2.x.

[37] Riseborough, P., "Using the ECL EKF," , Accessed Nov 2022. Retrieved from https://docs.px4.io/main/en/advanced_config.html.

[38] Caflisch, R. E., "Monte Carlo and quasi-Monte Carlo methods," *Acta Numerica*, 1998, pp. 1–49. https://doi.org/10.1017/S0962492900002804.

[39] Navarro, M., Witteveen, J., and Blom, J., "Polynomial Chaos Expansion for general multivariate distributions with correlated variables," *arXiv*, 2014. https://doi.org/10.48550/arXiv.1406.5483.

[40] Rahman, S., "A Polynomial Chaos Expansion in Dependent Random Variables," *Journal of Mathematical Analysis and Applications*, Vol. 464, No. 1, 2018, pp. 749–775. https://doi.org/10.1016/j.jmaa.2018.04.032.

[41] Gahan, K. C., Hopwood, J. W., and Woolsey, C. A., "Uncertainty in Wind Estimates, Part 2: H_∞ Filtering using Generalized Polynomial Chaos," *AIAA SCITECH 2024 Forum*, Orlando, FL, 2024. To Appear.